metals

MDPI

Article

Fatigue Behavior of Hybrid Components Containing Maraging Steel Parts Produced by Laser Powder Bed Fusion

Luís Santos [1], Joel de Jesus [1,*], Luís Borrego [1,2], José A. M. Ferreira [1], Rui F. Fernandes [1], José D. M. da Costa [1] and Carlos Capela [1,3]

[1] Department of Mechanical Engineering, Centre for Mechanical Engineering, Materials and Processes (CEMMPRE), University Coimbra, P-3004 516 Coimbra, Portugal; luis_lms@sapo.pt (L.S.); borrego@isec.pt (L.B.); martins.ferreira@dem.uc.pt (J.A.M.F.); uc2020158278@student.uc.pt (R.F.F.); jose.domingos@dem.uc.pt (J.D.M.d.C.); ccapela@ipleiria.pt (C.C.)

[2] Department of Mechanical Engineering, Coimbra Polytechnic–ISEC, Rua Pedro Nunes, 3030-199 Coimbra, Portugal

[3] Department of Mechanical Engineering, School Tech and Management, Polytechnic Institute of Leiria, 2411-901 Leiria, Portugal

* Correspondence: joel.jesus@uc.pt

Abstract: This investigation concerns about of fatigue behavior under controlled loading and under strain control for hybrid specimens with parts produced with conventional processes in steel AISI H13 and the stainless steel AISI 420 and the rest part produced by laser powder bed fusion in AISI 18Ni300 steel. The controlled loading tests were performed in constant and variable amplitude. Fatigue failure of hybrid samples occurs mostly in laser-melted parts, initiated around the surface, in many cases with multi-nucleation and propagated predominantly between the deposited layers. Fatigue strength of hybrid parts, tested under displacement control is similar, but for specimens tested under load control the fatigue strength the fatigue strength of hybrid specimens is progressively lesser than laser powder bed fusion samples. Despite a tendency to obtain conservative predictions, Miner's law predicts reasonably the fatigue lives under block loadings. The interface between materials presented an excellent joining and fatigue strength because the fatigue failure of hybrid samples occurred mostly in laser melted parts out of the interface.

Keywords: laser powder bed fusion; fatigue; functional materials; structural integrity

Citation: Santos, L.; de Jesus, J.; Borrego, L.; Ferreira, J.A.M.; Fernandes, R.F.; da Costa, J.D.M.; Capela, C. Fatigue Behavior of Hybrid Components Containing Maraging Steel Parts Produced by Laser Powder Bed Fusion. *Metals* **2021**, *11*, 835. https://doi.org/10.3390/met11050835

Academic Editors: Yongho Sohn and Sergey N. Grigoriev

Received: 8 April 2021
Accepted: 17 May 2021
Published: 19 May 2021

1. Introduction

Laser powder bed fusion (LPBF) is a technology of rapid manufacturing that builds metal parts layer by-layer using metal powders [1] fused by a high-power laser. This technique is increasingly used to obtain components with complex shapes namely in automotive, aerospace, medical and of injection molds industries. Several studies have been previous published on the area of LPBF technology using different metal powders, for example, the fabricating of iron-base alloys [2–5], nickel-base alloys [6,7], copper-base alloys [8] and titanium-base alloys [9].

LPBF components could present characteristic cast structure, with presence of porosity, high superficial roughness, non-homogeneous microstructure and thermal residual stresses due to the processing with extreme temperature gradients and the high cooling rates, inducing medium mechanical properties. However, additional post-processing treatments can improve these properties [10]. The mechanical properties of components produced by LPBF are mainly affected by above referred parameters, like the scan speed and layer thickness. The different parameters can be grouped in powder characteristics and processing parameters [11]. The occurrence of pores originated from initial powder contaminations, evaporation or local voids after powder-layer deposition is the major drawback in mechanical properties [12–14]. Especially under fatigue, pores can act as stress concentrators leading to easier failure [15].

Since LPBF is an additive manufacturing process with a layer-by-layer deposition, the phenomenon lack of fusion is an inhibitor to the uniform deposition of a fresh powder on the previously sintered layer. Therefore, this behavior tends to cause porosity and even delamination induced by reduced bonding between layers in combination with thermal stress [11,16–19]. This effect is a complex metallurgical process that is controlled by both laser processing conditions and powder material properties [20–23].

Mooney et al. [24] compiled the factors affecting the mechanical properties of maraging Steel 300 fabricated via LPBF, being that: the quality and the powder morphology can play an important role in the LPBF process in order to achieved higher relative density and optimizing mechanical properties; parameters of LPBF process affect directly the material microstructure and therefore they impact on the mechanical properties and anisotropie of the material; the build orientation influences the mechanical performance of the material and can be improved with heat treatments. Anisotropy can be drastically reduced via an appropriate choice of such plans, which are generally easy to implement for this material.

The influence of melting parameters and selection of metal powder on microstructure of the parts have been the main focus of a high number of studies on LPBF materials. These studies, state that for some materials, LPBF components are capable to achieve static mechanical properties comparable to the ones of conventionally produced parts from bulk materials [25]. Zitelli et al. [26] in their review showed that stainless steel alloys have been satisfactorily processed by LPBF process. The reached mechanical properties make stainless steels fit the requirements of numerous applications. High mechanical properties are achieved, since the porosity level achieved by LPBF is quite low and is comparable to conventionally produced materials.

In spite of, significant results recently published about fatigue behavior of steel LPBF parts [27,28], more research is needed, particularly for structural applications. Spierings et al. [29] investigated the S-N curves of two stainless steel types (316L and 15-5PH), focusing the objectives on the comparison of the results obtained from LPBF and conventionally processed materials, concluding that LPBF specimens exhibits comparable dynamic properties than conventionally processed parts. However, they obtained an important influence of the LPBF surface roughness on the fatigue strength, particularly for long fatigue lives. Branco et al. [30] studied the low cycle fatigue behavior of AISI 18Ni300 maraging steel produced LPBF concluding that the fatigue crack nucleated from the surface defects as: unmolten particles and zones with lack of fusion.

On the other hand, Bhaduri et al. [31] evaluated tensile mechanical properties and microstructure of hybrid specimens made from AlSi10Mg parts built by LPBF on AA6082 machined parts. The hybrid components failed under tension at their interface. These conditions enable building LPBF structures with <1% porosity. Recent work was produced by the authors about the mechanical properties of parts manufactured in AISI 18Ni300 steel produced by LPBF, including the fatigue behavior of LPBF specimens [32], hybrid components [33], fatigue crack propagation [34] and fracture toughness [35]. The results indicate that the fatigue strength is strongly affected by defects inherent to the LPBF process. Moreover, the failure sites of hybrid components occurred always in the parts produced by LPBF process.

The mold production or reparation by LPBF is a growing practice in the mold industry. In mold reparation by LPBF is often found hybrid parts because not all materials can be used in the LPBF process, therefore it becomes useful to study the mechanical properties in hybrid parts. The objective of this work was to investigate the fatigue performance of hybrid specimens obtained by LPBF maraging steel implants into hot working tools and stainless steels substrates. Since functional components can be manufactured by LPBF, it is necessary to warrant that final functional requirements are fulfilled by the components. For this purpose, were performed tensile tests, fatigue tests under constant amplitude and block loadings and fractography analysis. A detailed analysis was performed about the failure mechanisms and interfaces microstructures.

2. Materials and Methods

Experimental program, involving static and fatigue tests, was performed using round specimens. Two material batches of hybrid samples, in which one part was produced by LPBF and other part is a substrate steel, produced by conventional processes. Fatigue results were compared with previous work with LPFB specimens, produced only by LPBF technique. Figure 1 shows the geometry and dimensions of the hybrid specimens.

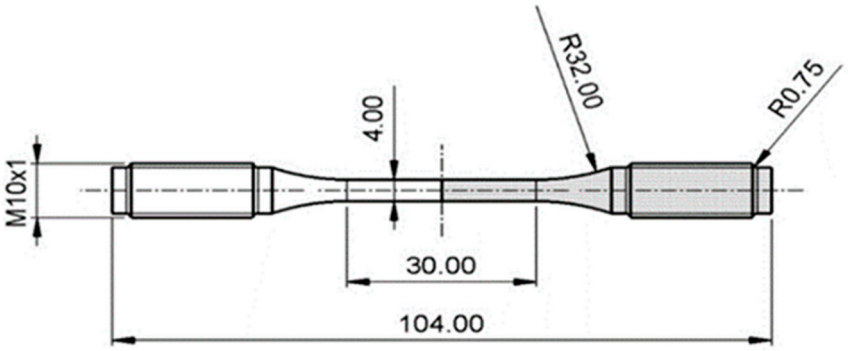

Figure 1. Geometry and dimensions of hybrid specimens.

Laser powder bed fusion (LPBF) was processed using a high-power laser to fuse steel powder particles layer by layer by Lasercusing®. The sample layers are deposited in planes perpendicular to the axial direction of the specimens. The equipment was of the mark "Renishaw" and model "AM 400". This machine is composed by a laser type Nd: YAG with a maximum power of 400 W in continuous wave mode and a wavelength of 1064 nm. Figure 2 shows a SEM image of transversal section being possible to visualize the route of the power melting.

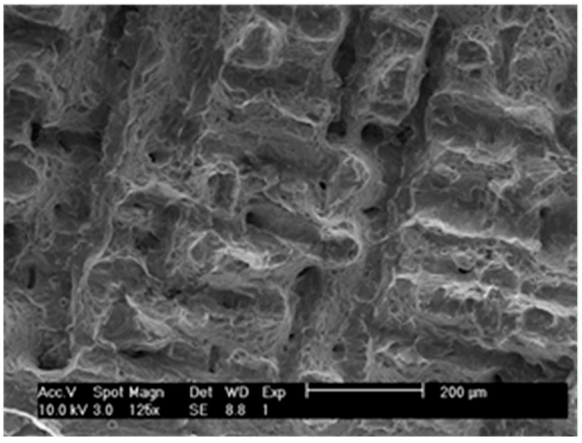

Figure 2. SEM image of melting route.

The scan speed of 200 mm/s was used for processing laser melting, resulting a deposited layer about 30 µm thickness [32]. The material of the powder particles was the maraging steel AISI 18Ni300. The choice of this steel was due to its high utilization in the molds production and reparation given that this steel conserves the mechanical properties in higher temperatures due to the high amount of nickel in its structure. The hybrid specimens were produced alternatively in two materials: the steel for hot work tools AISI H13 (HS) and the stainless steel AISI 420 (SS). Before testing all specimens were polished in order to reduced surface roughness. The average surface roughness in all specimens was about, R_z = 0.47 µm.

The scan speed of 200 mm/s was chosen after a detailed analysis by authors in previous work [32], where was studied the effect of the scan speed (the authors used 200,

400 and 600 mm/s) on the microstructure, defect level, density and mechanical properties. The defect level was based on microscopy analysis and by comparing density values. The better results were obtained with 200 mm/s scan speed, for which was obtained: a porosity of 0.74%, density of 7.42 g/cm^3, hardness of HV1 354, Young's Modulus of 168 GPa and a tensile strength of 1147 MPa.

The chemical composition, according with the manufacturers, is shown in Table 1. The sample code identifies the test series, corresponding to abbreviations of the materials used for each part. Table 2 show the material design composition of the two batches used in present study.

Table 1. Chemical composition of the materials.

Steel	C	Ni	Co	V	Mo	Ti	Al	Cr	P	Si	Mn	Fe
18Ni300	0.01	18.2	9.0	-	5.0	0.6	0.05	0.3	0.01	0.1	0.04	Balance
1.2344	0.40	-	-	0.94	1.30	-	-	5.29	0.017	1.05	0.36	Balance
1.2083	0.37	-	-	0.17	-	-	-	14.22	0.021	0.64	0.37	Balance

Table 2. Samples materials design.

Sample Code	Substrate Material	Implant Material
LPBF/HS	18Ni300 powder (LPBF)	1.2344 Hot working steel (HS)
LPBF/SS	18Ni300 powder (LPBF)	1.2083 Stainless steel (SS)

A 10 kN capacity Instron EletroPuls E10000 machine (Instron, Norwood, MA, USA) was used to perform both, tensile and fatigue tests. Tensile tests were carried out using a testing speed of 2 mm/min at room temperature. The fatigue tests were performed with a frequency of 15 Hz in tension, also at room temperature. Fatigue tests were carried out:

- Under constant amplitude loading two series of tests were performed: One in load control at constant amplitude sinusoidal load wave with stress ratio R = 0 and another in displacement control with zero minimum strain.
- Under variable amplitude tests using a reference block loading, composed by three blocks with stress ratio of R = 0, applied during 1000 of cycles for each block. The stress range applied during each block is schematically depicted in Figure 3.

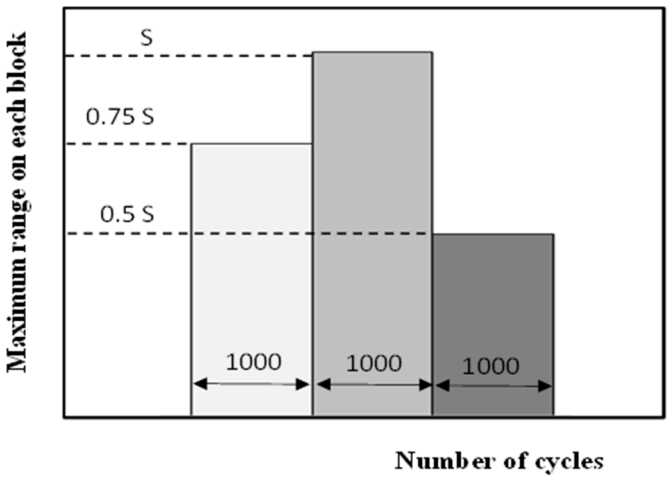

Figure 3. Schematic presentation of the block loadings.

An average of eight specimens were used for each series in order to create the curves of stress vs number of cycles at failure. It is important to notice that this study was conducted with limited number of specimens for each analyzed condition and therefore the obtained

results cannot be addressed as project data. However, the objective is to understand the fatigue behavior of the material hybrid samples, as well as to perform a detailed analysis about the failure mechanisms and interfaces micro-structures. Moreover, the test procedure agrees with the best practice in fatigue studies.

Microstructures were analyzed in LPBF material and interface regions. Therefore, hybrid specimens were cut in planes containing the axial axe of the specimens, polished and attacked Picral solution for two minutes (ethyl alcohol with 4% of picric acid solution), followed by a second attack for 20 s in a solution that results from Picral mixture with addition of 1% hydrochloric acid. After samples preparation, the microscope Leica DM4000 M LED (Leica Microsystems, Wetzlar, Alemanha) was used to make their observation. The fracture surfaces of some fatigue specimens were observed and analyzed by SEM using a scanning electron microscope Philips XL 30 (Philips, Eindhoven, The Netherlands). Figure 4a shows the microstructure into the LPBF material, presenting a good coherency between the elongated deposited layer with about 150 µm wide and about 30–35 µm width, the formation of cellular solidification structure and possible martensitic needles (red dashed line) [36] and a significant number of impurities result of the etching process. Hybrid samples interface region was analyzed in order to better understand the variations in microstructure and quality of adhesion. Figure 4b,c present the metallography in the longitudinal section interface region for a LPBF/HS and a LPBF/SS hybrid specimen, respectively. Both figures show corrugated regions in the substrate material, caused by melting in the first laser pass. In both cases there is an interface region on the substrate with a width of approximately 30–50 µm. In this region there is a significant microstructural change resulting from the high temperature and sudden cooling that occurred in the manufacturing process. Figure 4b presents a darker zone indicating a higher carbon concentration due to decarburization has occurred in the zone near the interface, which is indicated by the white colour of this region. On the other hand, Figure 4c shows that did not occurred decarburization in the interface zone. The presence of porosities was observed (marked by red arrows) in the LPBF material but were not observed at the specimens' interface. In both cases was verified an excellent cohesion between steels.

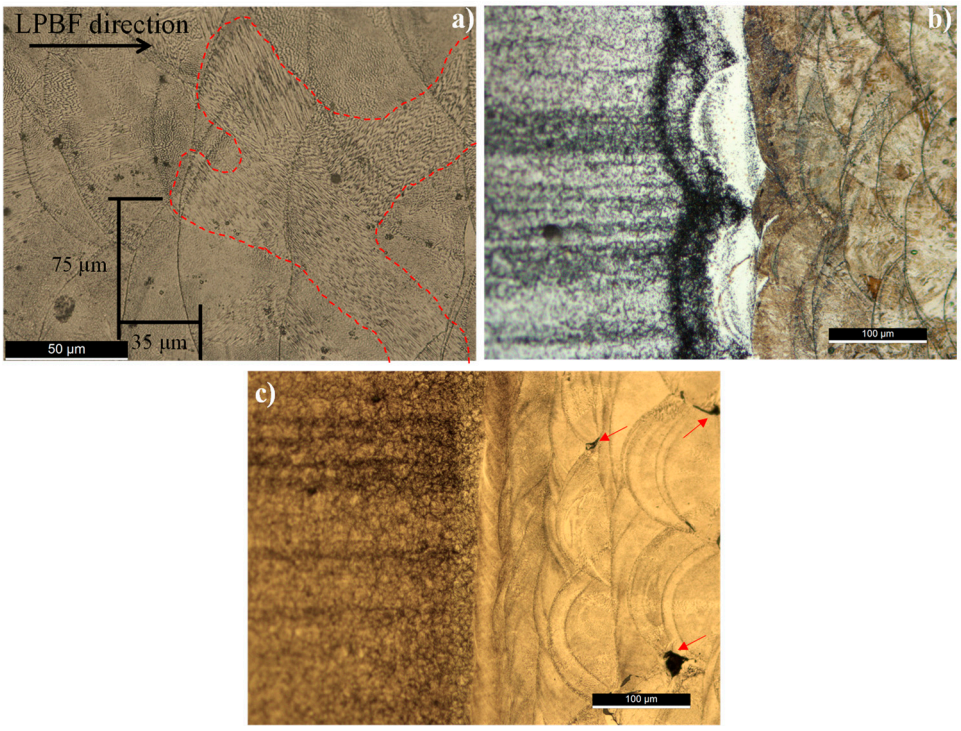

Figure 4. (**a**) Microstructure of LPBF material; (**b**) interface LPBF/HS specimen; (**c**) interface LPBF/SS specimen.

A Struers Duramin 1 microhardness tester was used to perform Vickers hardness testing according to ASTM E384-11e1 [37] at 0.5 mm between indentations with 1 kg load. Distance between indentations in interface region was only 0.25 mm. The following values were obtained for the three materials: 533.1 ± 6.17, 505.8 ± 2.75, 339.5 ± 8.60 HV1, for the AISI 420, AISI H13 steels and LPBF material, respectively. In the hybrid specimens, the transition between the typical hardness of the two materials occurs rapidly and progressively in a narrow band less than 2 mm wide.

3. Results and Discussion

Figure 5 shows representative load–displacement curves obtained for the different samples (were tested three samples for each series). It can be observed an initial linear region followed by a non-linear behavior typical of metallic materials. The hybrid samples have higher global stiffness than the LPBF only specimens, as a consequence of the recorded strain to be an average value in the region of the interface between the ends of the extensometer (12.5-gauge length). For hybrid specimens, this region includes two materials with different stiffness, LPBF material with lower Young's modulus, AISI 420 and AISI H13 steels with similar and higher Young's modulus. In opposite, strain at failure is lower for hybrid specimens. Failure stress is similar for the three batches of materials, because failure occurs in all cases in LPBF material sections. Ultimate strength was calculated from peak load of the load versus displacement curves. The Young's modulus was obtained by linear regression of the stress-strain curves considering the larger range corresponding to a correlation coefficient higher than 0.995. The values of the ultimate strength and the Young's modulus are summarized in Table 3.

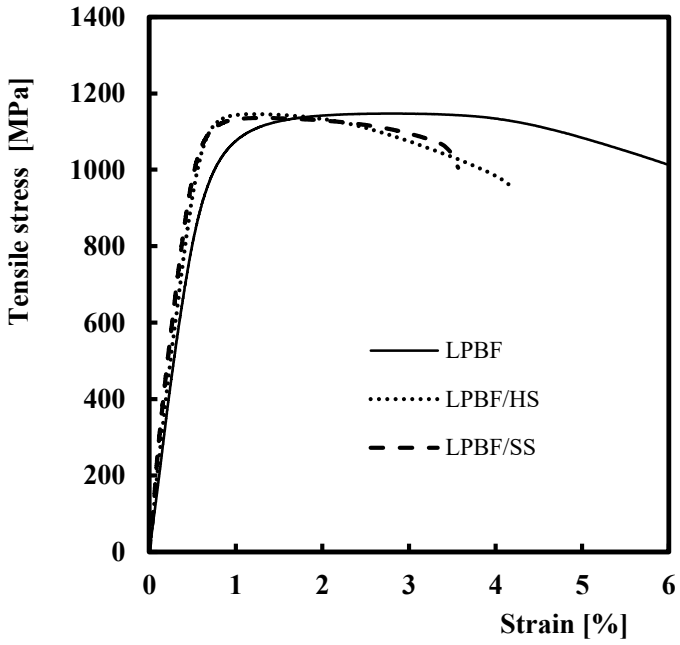

Figure 5. Exemplary tensile curves.

Table 3. Mechanical properties.

Sample Code	Young's Modulus, GPa	Tensile Strength, MPa	Strain at Failure, %
LPBF	168 ± 9	1147 ± 13	6.12 ± 0.001
LPBF/HS	181 ± 6	1139 ± 12	4.2 ± 0.03
LPBF/SS	173 ± 7	1144 ± 10	3.8 ± 0.08

Five batches of fatigue tests were performed: tests under load control for all the three types of samples and tests under displacement control for LPBF and LPBF/HS samples.

The pulsating tensile loading fatigue results were analyzed using the initial nominal stress range against the number of cycles to failure. Figure 6a,b compare the results obtained for the different specimen configurations, for the tests under load control and displacement control, respectively. The analysis of Figure 6a indicates that for longer lives, the fatigue strength of hybrid specimens is progressively less than that of the fully LPBF only samples, while Figure 6b shows that fatigue strength of LPBF only samples and hybrid LPBF/HS samples, tested under displacement control is similar. These results indicate that fatigue life of laser melting samples is controlled by strain range and the use of hybrid parts manufactured with AISI H13 and AISI 420 steels substrates do not affect significantly the fatigue strength. The effect of the substrate is a result: good adhesion in the interface above mentioned (as observed in Figure 4b,c, and the fact that the LPBF region is constitute itself as the weakest area in terms of fatigue resistance. On the other side, the results indicate that a small tendency to increasing fatigue life under displacement control in comparison with load control tests, which can be caused by the material softening observed by authors [34].

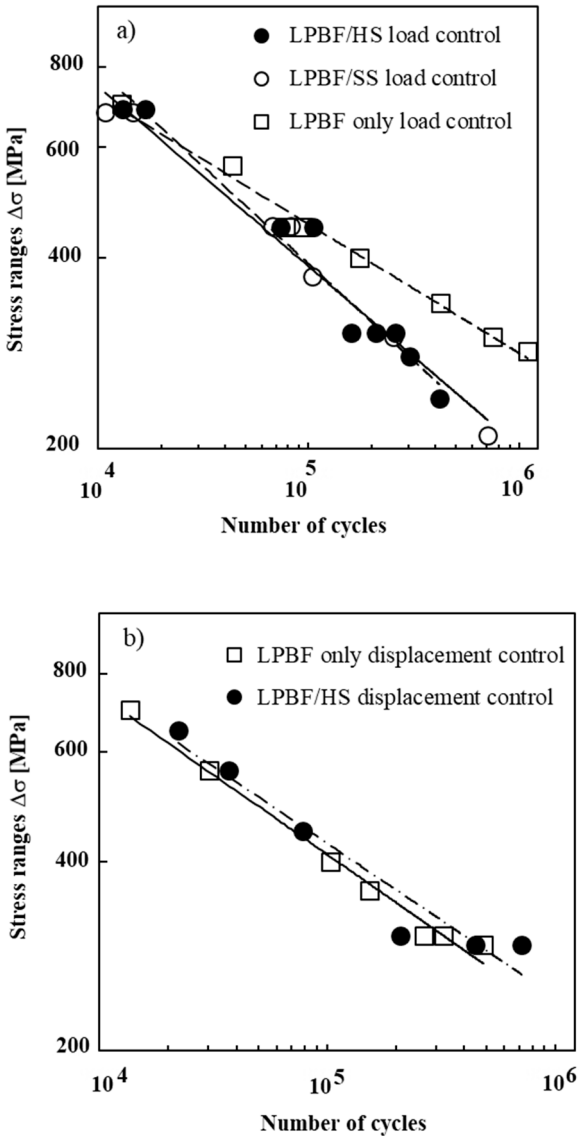

Figure 6. Curves of stress range vs number of cycles at failure; (**a**) load control; (**b**) displacement control.

The failure sites were observed and measured from the interface. Figure 7 shows a photo of a longitudinal section, positioning failure section in respect to interface on a

LPBF/HS sample. This figure is representative of failure positions, showing bulk HS steel, interface and failure section, which occurs always in LPBF material. Figure 8 depicts a histogram of the distance of the failure sections from the interface, providing evidence that most of the fractures occur at the LPBF regions. The reasons why these sintered parts are less resistant to nucleation and growth of fatigue cracks will be possible due the type of microstructure, lower microhardness, the presence of a significant number of small micro pores and positive residual stresses around surface in LPBF region. This event confirms good adhesion and metallurgic compatibility between materials of hybrid parts.

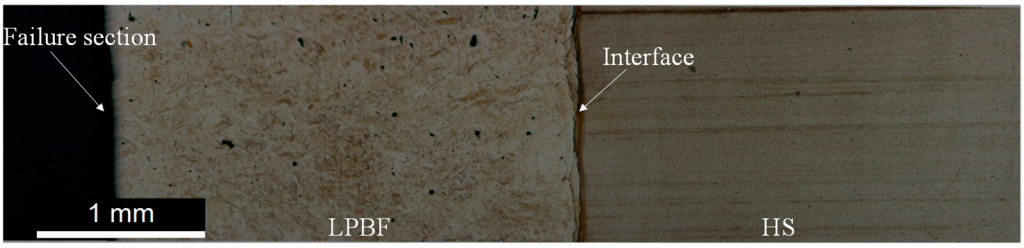

Figure 7. View of failure section in a LPBF/HS sample.

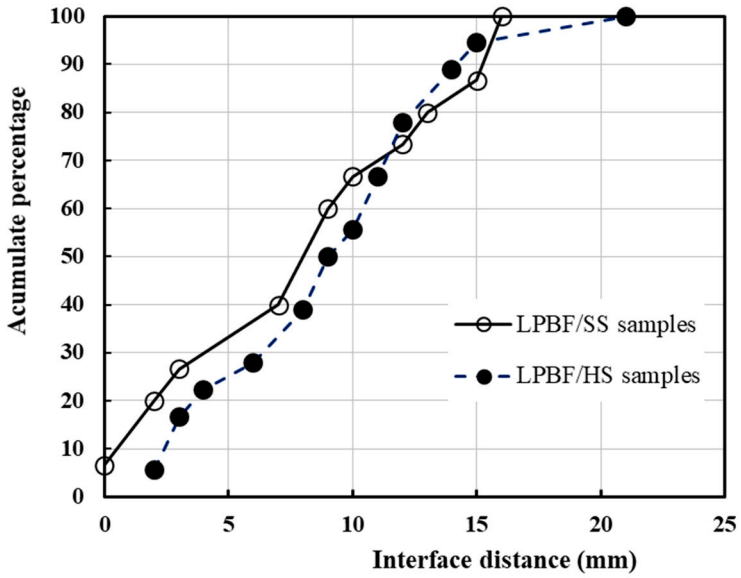

Figure 8. Histogram of failure section position.

Fracture surfaces were analyzed by scanning electron microscope, presenting Figure 9 some exemplary SEM images of the failure in only LPBF material. In spite of the presence of internal micro pores, and also the presence of positive residual stresses [34], fatigue crack initiated around the surface, in laser melted material and propagated through the cross section. As observed by the authors in previous work [32], in many cases, occurred surface multi-nucleation as shown in Figure 9a. Fatigue crack propagation occurs under mixed mode: predominantly between the deposed layers revealing the scan pattern (as shown in Figure 9b), and a transgranular failure through the deposited layer drive by the presence of microporosities and of impurities due to the etching process, as reveals a higher magnification observation, Figure 9c. The observation of the failure surface using 3D microscopy confirms the crack path, contouring the deposed layers and growing through the microporosities and impurities defects, as shown in Figure 9d.

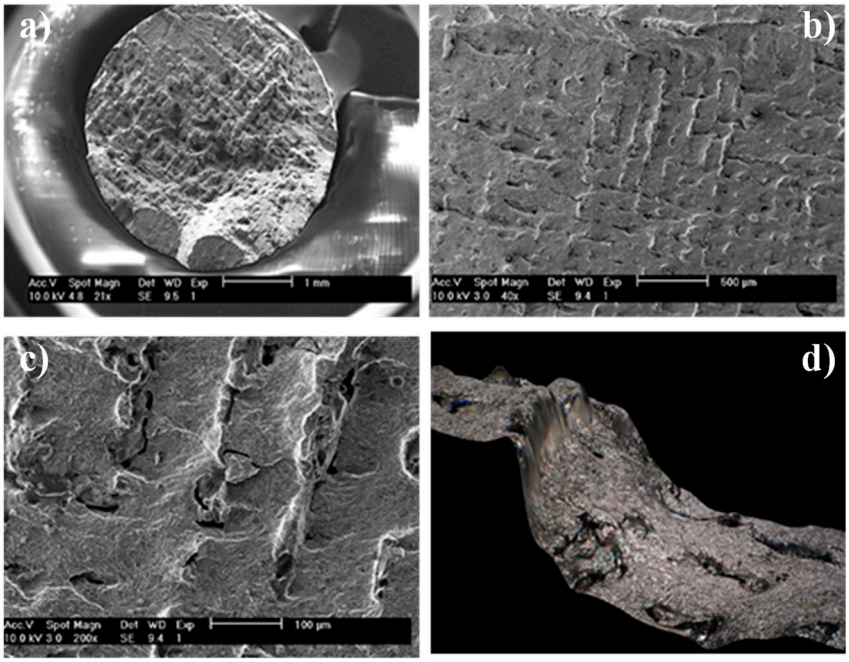

Figure 9. Images of surface fracture. (**a**) SEM image of fracture surface; (**b**) magnification of Figure 9a; (**c**) magnification of Figure 9b; (**d**) image of failure surface using 3D microscopy.

The fatigue results under variable amplitude loading were analyzed using the known Miner's law. Neglecting the existence of a fatigue limit, in Miner's rule enables the definition of an equivalent stress [38].

Figures 10 and 11 compare the predicted lives, Np, obtained by the Miner's law and the experimental results of the fatigue tests on variable amplitude of hybrid parts, Nf, for the samples LPBF/HS and LPBF/SS, respectively. In these figures the limits Np = 2Nf and Np = 0.5Nf were also plotted and used as a criterion of prediction exactness.

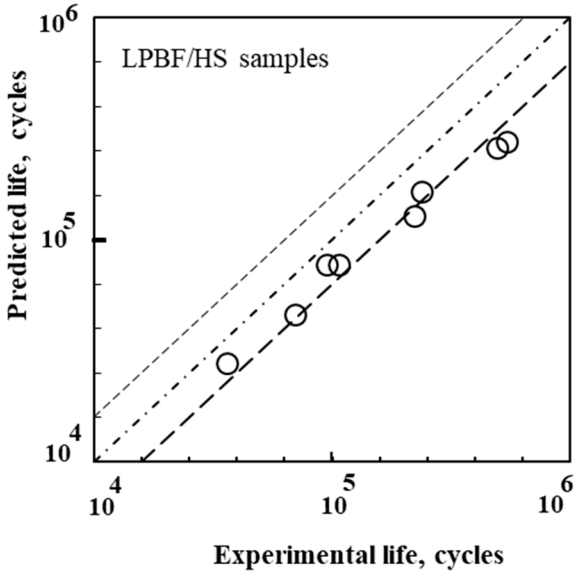

Figure 10. Predicted fatigue for variable amplitude loading. LPBF/HS samples.

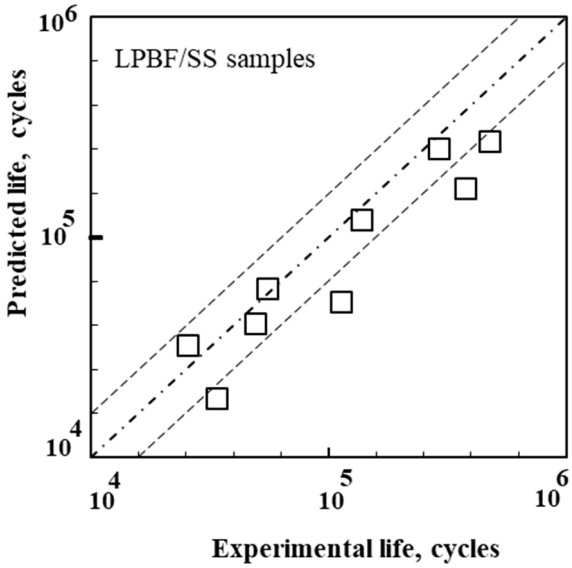

Figure 11. Predicted fatigue for variable amplitude loading. LPBF/SS samples.

A good agreement was obtained between the predicted lives and the experimental results, which is indicated by the presence of the results mainly between the two limits, which is usually considered as a correspondent for a very good agreement. From the analysis of this figure is can be concluded that Miner's law is adequate to predict fatigue life in hybrid components with sintered implants. However, particularly for the LPBF/SS specimens a tendency to be conservative was observed.

4. Conclusions

The main conclusions are:

- Tensile properties of only LPBF and hybrid specimens are quite similar. However, for the materials combinations studied hybrid parts have higher stiffness (+7%) and lower strain at failure (−61%).
- Fatigue failure of hybrid samples occurs in laser melted parts, once LPBF material exhibits lower crack initiation resistance as consequence of lower micro hardness, about of −70%, and the presence of a significant number of small micro pores. Fatigue cracks initiated around the surface, in many cases with multi-nucleation and propagated predominantly between the deposed layers or through the internal microporosities and impurities defects. The interface between materials showed an excellent connection and fatigue strength due to the fatigue failure of hybrid samples occurred frequently in laser melted parts out of the interface.
- For short lives, fatigue strength of LPBF and hybrid parts, tested under load control was quite similar. However, for long lives, the fatigue strength of hybrid specimens is progressively lesser than that of LPBF samples, for 500,000 cycles a loss of 52%. Fatigue strength of LPBF and hybrid parts, tested under displacement control is similar, suggesting that fatigue failure is controlled by the strain range.
- Miner's law provides good predictions of the fatigue lives under block loadings due to the ratio between the experimental and predicted fatigue life showed an error bellow to 10%, despite a tendency to obtain conservative predictions, particularly for the LPBF/SS specimens.

Author Contributions: Conceptualization, J.A.M.F. and L.B.; methodology, J.D.M.d.C.; software, J.d.J.; formal analysis, L.S. and J.d.J.; investigation, L.S., R.F.F. and J.d.J.; resources, C.C.; data curation, L.S. and J.d.J.; writing—original draft preparation, J.d.J.; writing—review and editing, L.B.; supervision, J.A.M.F. and J.D.M.d.C.; project administration, J.A.M.F.; funding acquisition, J.A.M.F. and L.B. All authors have read and agreed to the published version of the manuscript.

Funding: The authors would like to acknowledge the sponsoring under the project POCI-01-0247-FEDER-042536, financed by European Funds, through program COMPETE2020, under the Eureka smart label S0129-AddDies. This research is also sponsored by national funds through FCT—Fundação para a Ciência e a Tecnologia, under the project UIDB/00285/2020.

Data Availability Statement: The data presented in this study are available on request from the corresponding author. The data are not publicly available due to privacy.

Conflicts of Interest: The authors declare no conflict of interest.

References

1. Santos, E.C.; Shiomi, M.; Osakada, K.; Laoui, T. Rapid manufacturing of metal components by laser forming. *Int. J. Mach. Tools Manuf.* **2006**, *46*, 1459–1468. [CrossRef]
2. Simchi, A.; Pohl, H. Direct laser sintering of iron–graphite powder mixture. *Mater. Sci. Eng. A* **2004**, *383*, 191–200. [CrossRef]
3. Simchi, A. Direct laser sintering of metal powders: Mechanism, kinetics and microstructural features. *Mater. Sci. Eng. A* **2006**, *428*, 148–158. [CrossRef]
4. Kruth, J.P.; Froyen, L.; Van Vaerenbergh, J.; Mercelis, P.; Rombouts, M.; Lauwers, B. Selective Laser Melting of Iron-Based Powder. *J. Mater. Process. Technol.* **2004**, *149*, 616–622. [CrossRef]
5. Wang, Y.; Bergström, J.; Burman, C. Characterization of an iron-based laser sintered material. *J. Mater. Process. Technol.* **2006**, *172*, 77–87. [CrossRef]
6. Mumtaz, K.A.; Erasenthiran, P.; Hopkinson, N. High Density Selective Laser Melting of Waspaloy®. *J. Mater. Process. Technol.* **2008**, *195*, 77–87. [CrossRef]
7. Mumtaz, K.; Hopkinson, N. Top surface and side roughness of Inconel 625 parts processed using selective laser melting. *Rapid Prototyp. J.* **2009**, *15*, 96–103. [CrossRef]
8. Gu, D.; Shen, Y. Development and characterisation of direct laser sintering multicomponent Cu based metal powder. *Powder Met.* **2006**, *49*, 258–264. [CrossRef]
9. Osakada, K.; Shiomi, M. Flexible manufacturing of metallic products by selective laser melting of powder. *Int. J. Mach. Tools Manuf.* **2006**, *46*, 1188–1193. [CrossRef]
10. Maleki, E.; Bagherifard, S.; Bandini, M.; Guagliano, M. Surface post-treatments for metal additive manufacturing: Progress, challenges, and opportunities. *Addit. Manuf.* **2021**, *37*, 101619. [CrossRef]
11. Simchi, A.; Petzoldt, F.; Pohl, H. Direct metal laser sintering: Material considerations and mechanisms of particle: Rand tooling of powdered metal parts. *Int. J. Powder Metall.* **2001**, *37*, 49–61.
12. Murr, L.E.; Gaytan, S.M.; Ceylan, A.; Martinez, E.; Martinez, J.L.; Hernandez, D.H.; Machiado, B.I.; Ramirez, D.A.; Medina, F.; Collins, S.; et al. Characterization of titanium aluminide alloy components fabricated by additive manufacturing using electron beam melting. *Acta Mater.* **2010**, *58*, 1887–1894. [CrossRef]
13. Gorny, B.; Niendorf, T.; Lackmann, J.; Thoene, M.; Troester, T.; Maier, H.J. In situ characterization of the deformation and failure behaviour of non-stochastic porous structures processed by selective laser melting. *Mater. Sci. Eng. A* **2011**, *528*, 7962–7967. [CrossRef]
14. Vilaro, T.; Colin, C.; Bartout, J.-D. As-Fabricated and Heat-Treated Microstructures of the Ti-6Al-4V Alloy Processed by Selective Laser Melting. *Met. Mater. Trans. A* **2011**, *42*, 3190–3199. [CrossRef]
15. Brandl, E.; Heckenberger, U.; Holzinger, V.; Buchbinder, D. Additive manufactured AlSi10Mg samples using Selective Laser Melting (SLM): Microstructure, high cycle fatigue, and fracture behavior. *Mater. Des.* **2012**, *34*, 159–169. [CrossRef]
16. Zhu, H.H.; Lu, L.; Fuh, J.Y.H. Study on Shrinkage Behaviour of Direct Laser Sintering Metallic Powder. *Proc. Inst. Mech. Eng. Part B J. Eng. Manuf.* **2006**, *220*, 183–190. [CrossRef]
17. Chatterjee, A.N.; Kumar, S.; Saha, P.; Mishra, P.K.; Choudhury, A.R. An experimental design approach to selective laser sintering of low carbon steel. *J. Mater. Process. Technol.* **2003**, *136*, 151–157. [CrossRef]
18. Murali, K.; Chatterjee, A.N.; Saha, P.; Palai, R.; Kumar, S.; Roy, S.K.; Mishra, P.K.; Choudhury, A.R. Direct selective laser sintering of iron–graphite powder mixture. *J. Mater. Process. Technol.* **2003**, *136*, 179–185. [CrossRef]
19. Dingal, S.; Pradhan, T.R.; Sarin Sundar, J.K.; Choudhury, A.R.; Roy, S.K. The application of Taguchi's method in the experimental investigation of the laser sintering process. *Int. J. Adv. Manuf. Technol.* **2008**, *38*, 904–914. [CrossRef]
20. Gu, D.; Shen, Y. Balling phenomena in direct laser sintering of stainless steel powder: Metallurgical mechanisms and control methods. *Mater. Des.* **2009**, *30*, 2903–2910. [CrossRef]
21. Niu, H.J.; Chang, I.T.H. Instability of scan tracks of selective laser sintering of high speed steel powder. *Scripta Mater.* **1999**, *41*, 1229–1234. [CrossRef]
22. Tolochko, N.K.; Mozzharov, S.E.; Yadroitsev, I.A.; Laoui, T.; Froyen, L.; Titov, V.I.; Ignatiev, M.B. Balling processes during selective laser treatment of powders. *Rapid Prototyp. J.* **2004**, *10*, 78–87. [CrossRef]
23. Das, S. Physical Aspects of Process Control in Selective Laser Sintering of Metals. *Adv. Eng. Mater.* **2003**, *5*, 701–711. [CrossRef]
24. Mooney, B.; Kourousis, K. A Review of Factors Affecting the Mechanical Properties of Maraging Steel 300 Fabricated via Laser Powder Bed Fusion. *Metals* **2020**, *10*, 1273. [CrossRef]

25. Abe, F.; Osakada, K.; Shiomi, M.; Uematsu, K.; Matsumoto, M. The manufacturing of hard tools from metallic powders by selective laser melting. *J. Mater. Process. Technol.* **2001**, *111*, 210–213. [CrossRef]
26. Zitelli, C.; Folgarait, P.; Di Schino, A. Laser Powder Bed Fusion of Stainless Steel Grades: A Review. *Metals* **2019**, *9*, 731. [CrossRef]
27. Wang, Y.; Bergström, J.; Burman, C. Four-point bending fatigue behaviour of an iron-based laser sintered material. *Int. J. Fatigue* **2006**, *28*, 1705–1715. [CrossRef]
28. Leuders, S.; Thöne, M.; Riemer, A.; Niendorf, T.; Tröster, T.; Richard, H.A.; Maier, H.J. On the mechanical behaviour of tita-nium alloy TiAl6V4 manufactured by selective laser melting: Fatigue resistance and crack growth performance. *Int. J. Fatigue* **2013**, *48*, 300–307. [CrossRef]
29. Spierings, A.; Starr, T.; Wegener, K. Fatigue performance of additive manufactured metallic parts. *Rapid Prototyp. J.* **2013**, *19*, 88–94. [CrossRef]
30. Branco, R.; Costa, J.D.M.; Berto, F.; Razavi, S.M.J.; Ferreira, J.A.M.; Capela, C.; Santos, L.; Antunes, F. Low-Cycle Fatigue Behaviour of AISI 18Ni300 Maraging Steel Produced by Selective Laser Melting. *Metals* **2018**, *8*, 32. [CrossRef]
31. Bhaduri, D.; Penchev, P.; Essa, K.; Dimov, S.; Carter, L.N.; Pruncu, C.I.; Pullini, D. Evaluation of surface/interface quality, microstructure and mechanical properties of hybrid additive-subtractive aluminium parts. *CIRP Ann.* **2019**, *68*, 237–240. [CrossRef]
32. Santos, L.; Ferreira, J.; Jesus, J.; Costa, J.; Capela, C. Fatigue behaviour of selective laser melting steel components. *Theor. Appl. Fract. Mech.* **2016**, *85*, 9–15. [CrossRef]
33. Santos, L.; Ferreira, J.; Costa, J.; Capela, C. Fatigue Performance of Hybrid Steel Samples with Laser Sintered Implants. *Procedia Eng.* **2016**, *160*, 143–150. [CrossRef]
34. Santos, L.; Borrego, L.; Ferreira, J.; De Jesus, J.; Costa, J.; Capela, C. Effect of heat treatment on the fatigue crack growth behaviour in additive manufactured AISI 18Ni300 steel. *Theor. Appl. Fract. Mech.* **2019**, *102*, 10–15. [CrossRef]
35. Santos, L.M.S.; De Jesus, J.; Ferreira, J.M.; Costa, J.D.; Capela, C. Fracture Toughness of Hybrid Components with Selective Laser Melting 18Ni300 Steel Parts. *Appl. Sci.* **2018**, *8*, 1879. [CrossRef]
36. Yao, Y.; Huang, Y.; Chen, B.; Tan, C.; Su, Y.; Feng, J. Influence of processing parameters and heat treatment on the mechanical properties of 18Ni300 manufactured by laser based directed energy deposition. *Opt. Laser Technol.* **2018**, *105*, 171–179. [CrossRef]
37. ASTM E384-11e1. *Standard Test Method for Knoop and Vickers Hardness of Materials*; ASTM International: West Conshohocken, PA, USA, 2011. [CrossRef]
38. Miner, M.A. Cumulative Damage in Fatigue. *J. Appl. Mech.* **1945**, *12*, A159–A164. [CrossRef]